HHS Public Access

Author manuscript

Magn Reson Med. Author manuscript; available in PMC 2017 March 01.

Published in final edited form as:

Magn Reson Med. 2016 March ; 75(3): 1100–1109. doi:10.1002/mrm.25686.

Correction and optimization of a T2-based approach to map blood oxygenation in small cerebral veins

Lisa C. Krishnamurthy[1,2], **Deng Mao**[1], **Kevin S. King**[3], and **Hanzhang Lu**[1,3]

[1]Advanced Imaging Research Center, University of Texas Southwestern Medical Center, Dallas, TX, USA

[2]Department of Biomedical Engineering, University of Texas at Arlington, Arlington, TX, USA

[3]Department of Radiology, Johns Hopkins University, Baltimore, MD, USA

[4]Department of Radiology, University of Texas Southwestern Medical Center, Dallas, TX, USA

Abstract

Purpose—Cerebral venous blood oxygenation (Y_v) is an important biomarker in brain physiology and function. The present study proposes a procedure to provide a quantitative map of the brain's intravascular Y_v.

Theory—The method is based on a pulse sequence, T_2-Relaxation-Under-Phase-Contrast (TRUPC) MRI, with post-processing approaches to correct eddy-current effects.

Methods—A complete scan protocol consists of four TRU-PC scans sensitized to large and small vessels with anterior-posterior and foot-head flow-encoding directions, and the data are analyzed conjunctively. Eddy-current correction was performed by fitting the tissue phase to a hyperplane, and then subtracting the eddy-current phase from the measured vessel phase. The reproducibility of the Y_v-maps was examined in five participants. Sensitivity of the Y_v map to a caffeine challenge was studied in another five participants.

Results—Removal of eddy-current induced artifact allowed for the correction of T_2 measurements, as demonstrated in vivo and with simulation. A Y_v-map depicting all vessels in the slice can be obtained with the proposed protocol. Test-retest variability of the Y_v-map was 3.7±1.2%. Y_v reduction can be reliably detected (P<0.001) following the caffeine ingestion.

Conclusion—With the proposed TRU-PC protocol and eddy-current correction procedure, an accurate, vessel-specific Y_v map of the human brain can be obtained.

Keywords

blood oxygen saturation; small vessel; TRU-PC; eddy-currents; $CMRO_2$

Corresponding author: **Name:** Hanzhang Lu, Ph.D. **Affiliations:** Department of Radiology, Johns Hopkins University **Mailing Address:** 600 N. Wolfe Street, Park 322 Baltimore, MD 21287 **Office Phone:** 410-955-1431 **Office Fax:** 410-614-1977 hanzhang.lu@jhu.edu.

Introduction

The brain is a highly energetic organ, utilizing significant fractions of oxygen under basal conditions (1). Alterations in oxygen utilization have been noted in healthy ageing (2-4), and in diseases such as Mild Cognitive Impairment (5), Multiple Sclerosis (6), and addiction (7). One important facet to quantifying brain oxygen metabolism is the reliable measurement of venous blood oxygen saturation (Y_v) (8). Several MRI approaches have been proposed to measure blood oxygen saturation non-invasively (9-26). One line of these methods is based on a calibratable relationship between blood T_2 and Y_v (9,10,14,27,28). That is, one can measure the blood T_2 in vivo, and then convert the blood T_2 to Y_v with a known calibration plot (29).

Most oximetry techniques measure the blood oxygenation on a whole brain level at the posterior portion of the superior sagittal sinus. The Y_v measurements in "only" large vessels lack a certain spatial specificity because of blood mixing as it travels down the vascular path. The Y_v measured in a particular vascular segment will represent the oxygen saturation from blood entering the vasculature at that point, along with contributions from previous vascular segments. This "washout" effect in large vessel scans averages aberrant Y_v values from affected regions with normal Y_v values from other regions, such that disease-related changes in physiology are difficult to detect, motivating us to image small veins.

Recently, a non-invasive method exploiting this principle to examine vessel-specific Y_v in the brain, named T_2-Relaxation-Under-Phase-Contrast (TRU-PC) MRI, was reported (13,30). TRU-PC uses Phase Contrast (PC) MRI to separate pure blood signal from the surrounding static tissue (31-33), and a CPMG T_2-preparation (34,35) to measure blood T_2, which is converted to Y_v. TRU-PC MRI has been shown to provide reliable assessment of oxygenation in major veins, including the superior sagittal sinus, straight sinus, great vein, and internal cerebral vein (13,30). In this way, TRU-PC of large vessels is able to look at regional variations of oxygen extraction fraction throughout the brain, but may still suffer from the "washout" effect in large vessel scans. Thus, the mapping of oxygenation in small cortical veins, though not yet well established, may provide region-specific metabolic information.

In the present report, we aim to optimize TRU-PC acquisition and analysis procedures to map the oxygenation of the entire mid-sagittal vasculature, including both the small draining veins (1-2mm in diameter) and the major veins. In order to effectively measure blood signal with a large range of flow velocities and directions, four TRU-PC scans with two cutoff velocities (V_{enc}) and two flow-encoding directions are performed and their data are conjunctively analyzed. We found that the strong flow-encoding gradients required to image the small veins resulted in spurious signals in static tissue. Therefore, we conducted optimization and correction of the TRU-PC technique for accurate Yv evaluation in small, slow-flowing veins. To mitigate eddy-current effects induced by the flow-encoding gradients (which are particularly pronounced in low V_{enc} scans) we implemented a correction algorithm and demonstrated that the correction improves the accuracy of blood T_2 estimation. Test-retest reproducibility of the maps is quantified. Finally, we show that the vessel-specific Y_v maps are sensitive to physiological changes with a caffeine challenge.

Theory

Detrimental effects of eddy-currents on PC MRI

PC MRI requires two separate scans, in each of which a bipolar gradient is used to encode flow information. The polarity of the gradient is usually reversed between the two scans. PC MRI relies on the assumption that positive and negative lobes of the velocity encoding gradient have identical areas-under-curve (Figure 1a), so that no net phase will be obtained for a stationary spin (Figure 1c). However, in the presence of gradient-induced eddy-currents (Figure 1b), this is no longer the case. A net phase is added to both stationary and moving spins (Figure 1d) (36).

Eddy-currents are generated during the "switching" of the bipolar gradients, and their magnitudes are determined by how fast and large the switching is (since eddy-currents are opposing the flux of the changing magnetic field). To image the low blood velocity flowing through a small vessel, large gradients must be employed, with a high slew rate to minimize echo times (TE). Thus, the eddy-currents in a low Venc scan will be larger in magnitude than the eddy-currents generated in a high Venc scan.

Figures 1e and f illustrate how eddy-currents affect the MR data measured in PC MRI. The total signal acquired from each scan (Z_1 and Z_2) is the vector addition from both blood (orange vector in Figure 1e) and tissue (blue), but the resulting (ideal) Complex-Difference (CD) only contains contribution from blood (Figure 1e). However, if eddy-currents are present (Figure 1f), the CD includes additional signal sources. In the example illustrated in Figure 1f, the amplitude of CD is increased, but it could also be decreased. The phase difference between Z_1 and Z_2, $\Delta\phi$, is also effected because it contains an additional tern, $\Delta\varepsilon$, associated with the eddy-currents. The magnitude of the vectors Z_1 and Z_2 are not affected by the eddy-currents.

In TRU-PC, the blood T2 is calculated from the CD images, which ideally only contain blood signal. However, in the presence of eddy-currents, spurious tissue signal can also contribute to the CD image, which will affect the quantified T2. Whether the T2 is under or overestimated depends on the sign of the eddy-current induced phase relative to the sign of the blood phase. When the eddy-current induced phase $\Delta\varepsilon$ is positive, the T_2 is overestimated, and when $\Delta\varepsilon$ is negative, the T_2 is underestimated. This is because, when $\Delta\varepsilon$ is positive, the eddycurrent induced tissue signal contribution is of the same sign as the blood signal. Since the tissue T_2 is longer than venous blood T_2 at 3T (28), the measured T_2 becomes greater. The opposite is true when $\Delta\varepsilon$ is negative.

Correction of eddy-current effects

Let us define the additional phase difference caused by eddy-currents as:

$$\Delta\varepsilon = \Delta\phi_{measured} - \Delta\phi_{true} \quad [1]$$

where measured $\delta\varphi_{measured}$ is the measured phase difference between Z_1 and Z_2; true $\delta\varphi_{true}$ is the true phase difference. Therefore, once $\Delta\varepsilon$ can be estimated, we will be able to obtain true $\delta\varphi_{true}$. It is important to note that, although $\Delta\varepsilon$ is defined upon the total signal vectors,

Z_1 and Z_2, its amplitude is approximately the same as that of the tissue and blood components (Figure 1f). In other words, the eddy-current induced phase errors are the same in tissue and in blood such that,

$$\Delta\varepsilon=\Delta\varepsilon_{tissue}=\Delta\varepsilon_{blood} \quad [2]$$

Fortunately, the effects of eddy-currents on tissue, $\delta\varepsilon_{tissue}$, are relatively easy to estimate since $\Delta\varphi_{true,tissue} = 0$ Thus, from Eq. [1], we have

$$\Delta\varepsilon_{tissue}=\Delta\phi_{measured,tissue} \quad [3]$$

Therefore, one can use $\delta\varphi_{measured}$ image and mask it to only preserve the tissue voxels. One can then fit $\delta\varphi_{measured}$ spatially to a hyperplane, similar to methods previously developed by Langham, et al. to remove field-inhomogeneities in gradient-echo images (37). Briefly, $\delta\varphi_{measured}$ in tissue is modeled to have contributions from six different field terms.

$$\Delta\phi_{measured,tissue}=c_1+c_2X+c_3Y+c_4XY+c_5X^2+c_6Y^2 \quad [4]$$

in which the coefficients c_1 to c_6 describe the amount of contribution from each of the 0th order, 1st order, and 2nd order terms, (1, *X*, *Y*,...Y^2), and are determined by least squares fitting. The data from all effective TE (eTE) values are fitted conjunctively as their eddy-currents effects are identical.

Then, for any vessel voxels, $\Delta\varepsilon$ can be estimated from the corresponding values on the hyperplane and can be used to compute $\Delta\varphi_{true} = \delta\varphi_{measured} - \delta\varepsilon$. The corrected CD can be calculated using the law of cosines (38):

$$CD=\sqrt{|Z_1|^2+|Z_2|^2-2|Z_1||Z_2|cos\,(\Delta\phi)} \quad [5]$$

which can be fitted as a function of eTE to obtain blood T_2. Note again, that the magnitude of the vectors Z_1 and Z_2 are not affected by the eddy-currents, thus they do not need to be corrected (only $\Delta\varphi$ needs to be corrected for eddy-current effects).

Numerical simulation of the effects of eddy-currents on T_2 estimation

To assess the effects of eddy-currents on the measured T_2 from a theoretical perspective, numerical simulation was performed in which the bias in T_2,$\delta T_2 = T_{2,measured\ blood} - T_{2,true\ blood}$, was calculated as a function of $\Delta\varepsilon$. The Z_1 and Z_2 vectors were simulated by assuming a blood volume fraction of 0.2 and a tissue fraction of 0.8, with the following parameters, $T_{2,tissue}$=95ms (39), $T_{1,tissue}$=1200ms (39), $T_{2,blood}$=75ms (29), $T_{1,blood}$=1600ms (40). The flow-encoding gradients were assumed to generate a true,blood $\Delta\varphi_{true,blood}$ of 180° in the blood compartment (using a Venc=5 cm/sec). The relationship between ΔT_2 and $\Delta\varepsilon$ is represented with a 2D plot and the simulation results were compared to experimental data.

Materials and Methods

General

Experiments were performed on a total of 10 healthy subjects (age 29±6 years, range 21-40, 6 Males) using a 3 Tesla MRI scanner (Philips Healthcare, Best, The Netherlands). The protocol was approved by the local Institutional Review Board. The body coil was used for RF transmission, and a 32-channel head coil was used for receiving.

MRI experiment

To capture the complete mid-sagittal cerebral vasculature, four separate TRU-PC scans were employed: two scans sensitized to the small vessels, and two scans sensitized to the large vessels. One small-vessel scan was acquired with flow-encoding in Anterior-Posterior (AP) direction, while the other small-vessel scan was acquired with flow encoding in Foot-Head (FH) direction. This covered all possible vessels with sagittal in-plane flow. The two large-vessel scans were also acquired in AP and FH. The MR protocols for the large-vessel and small-vessel scans were similar, but with differences in flow-encoding cut-off velocity (Venc) ($Venc_{large}$=15cm/s (30), $Venc_{small}$=3cm/s for Male, and 5cm/s for Female). The slight difference in $Venc_{small}$ between male and female was due to gender differences in blood flow (2,3).

The general imaging parameters applicable to all TRU-PC scans were as follows: single 2D slice, FOV=200×200mm^2, Acquisition matrix=276×83, in-plane acquisition voxel size=0.72×2.41mm^2, Reconstruction matrix=400×400, slice thickness=5mm, single k-line acquisition per TR; T_2-preparation module used composite block pulses (90x-180y-90x) with τ_{CPMG}=10ms and MLEV-16 phase-cycling scheme (41); two effective TEs (eTE=0 and 40ms) were used. A shortest possible TE was used, which ranged from 5.0ms to 7.2ms depending on Venc and encoding direction. The total scan time for all four scans was 13min and 20sec (2min 50sec for each large vessel scan, and 3min 50sec for each small vessel scan). The TRU-PC data was exported from the scanner as complex images.

Prior to the TRU-PC scans, a Susceptibility Weighted Image (SWI) (42) was also acquired to guide the selection of veins. The SWI protocol was as follows: 3D gradient echo readout, sagittal orientation, AP phase encoding, read-out BW=80Hz, FOV=200×200mm^2, acquisition matrix = 400x333, reconstruction matrix=400×400, Sensitivity Encoding (SENSE) reduction factor = 2 (43) in Posterior direction, 13 slices, slice thickness=2mm, slice gap=0mm, TR=40ms, TE=25ms, FA=20°, scan duration=1:23min.

In five of the participants, the above-described protocol was performed twice to examine the test-retest reproducibility of the results. In the other five participants, the protocol was repeated following the ingestion of a 200mg caffeine tablet (NoDoz®, Novartis Consumer Health, Inc., New York, NY, USA) to test the sensitivity of the proposed protocol to known vascular challenges. The subjects were scanned before and after the ingestion of 200mg caffeine. Though caffeine is known to lower baseline Y_v by reducing the cerebral blood flow via vasoconstriction (44), the V_{enc} of the TRU-PC acquisition was not changed for the caffeine scanning session. Between sessions, the subjects were removed from the MRI scanner. Repositioning of the subject occurred exactly 60min after ingestion of caffeine.

Image processing

From the original complex images Z_1 and Z_2, three new images were computed: the magnitude of Z1 ($|Z_1|$) the magnitude of Z2 ($|Z_2|$), and the phase difference ($\Delta\varphi_{measured}$). Then, for estimation of blood T_2 without eddy-current correction, one can simply calculate the pure blood signal using Eq. [5] for each eTE value and fit the blood signal as a function of eTE.

For estimation of blood T_2 with eddy-current correction, additional processing steps were used. We first estimated the eddy-current induced phase difference, $\Delta\varepsilon$, as described in the Theory section. This was performed by fitting the measured tissue voxel phase, $\Delta\varphi_{measured,tissue}$, to a hyperplane using Eq. [4]. Note that voxels containing vessels should be removed from the image before fitting. This was carried out using the SWI image. Specifically, the SWI data was first processed using the Signal Processing in NMR (SPIN) software (MRI Institute for Biomedical Research, Detroit, MI) and in-house Matlab scripts to generate a minimum intensity projection (mIP) SWI image. With SPIN, the SWI phase image was high-pass filtered (64×64 Hamming), and a "phase mask" was created as described in Reference (45). The phase mask was multiplied with the magnitude image five times to enhance the veins. A minimum intensity projection (mIP) across the four center SWI slices was used for the remaining processing in Matlab. To create the tissue mask, the voxels with signal intensity <25% of maximum intensity (presumably veins) as well as its immediately adjacent voxels (less than three voxels in distance) were excluded. Voxels with high signal intensity (>10% maximum signal) in large vessel PC MRI and the immediately adjacent voxels (less than three voxels in distance) were also excluded.

Once the eddy-current induced phase difference $\delta\varepsilon$ was obtained, $\Delta\varphi_{measured}$ could be corrected to yield $\Delta\varphi_{true}$. Then, Eq. [5] could again be used to calculate the corrected pure blood signal, from which corrected blood T_2 could be estimated.

A blood T_2 map was generated in which only voxels that were identified as venous voxels in SWI had meaningful values. All other voxels in the map were set to be zero. For each venous voxel, the four data sets using large and small vessel Venc and AP and FH flow-encoding directions were averaged if they meet the signal inclusion thresholds. Specifically, if the SNR of the blood signal was greater than 4 and the phase difference $\Delta\varphi$ was greater than 0.05 radians, then the data from that scan was included in averaging. To improve signal stability in the voxel-wise map, the signal from neighboring non-zero voxels was averaged in an 8.5 mm radius (35 × 35 voxel kernel), and subsequently used in the T_2-fitting. The T_2 was then converted to Y_v using a known calibration plot (29), assuming a hematocrit of 41% (46).

Statistical and quantitative analysis

To quantitatively examine the effect of eddy-current correction on the T_2 estimation, region-of-interest (ROI) analysis was performed in the five subjects who underwent reproducibility study. This analysis focused on the small-vessel TRU-PC data as their eddy-currents are more prominent. Five ROIs were drawn in each data set, generating a total of 50 data points (5 subjects × 5 ROIs × 2 repetitions). The T_2 values before and after eddy-currents

correction were compared with a paired t-test. Furthermore, we examined the relationship between $\Delta T_2 (= T_{2,uncorrected} - T_{2,corrected})$ and $\Delta\varepsilon$ in a 2D scatter plot, and compared this result to the simulation result. This analysis was carried out separately for AP and FH flow encoding directions.

To further demonstrate that eddy-current correction improves the accuracy of Y_v estimation in small veins, we used large vessel Y_v as a reference, with the assumption that small vessel Y_v should be similar to the large vessel that it joins. Specifically, a small vessel ROI was drawn on the small vessel scan, and an adjacent large vessel ROI was drawn on the large vessel scan. A total of 10 adjacent large-vessel-small-vessel ROIs were drawn (5 from Anterior-Posterior scans, 5 from Foot-Head scans). Scatter plot between small and large vessel Y_v was examined, separately for uncorrected and corrected data. We hypothesized that the two types of vessels should show a better correspondence of Y_v in the corrected data. To increase the dynamic range of data, this analysis was performed on the caffeine challenge images.

The reproducibility of the method was assessed by calculating a voxel-wise Coefficient of Variation (CoV) (47) for all voxels designated as veins. The effect of caffeine was assessed by comparing the difference between baseline and caffeine Y_v-maps on a voxel-by-voxel basis, and with t-statistic.

Results

Eddy-currents correction in TRU-PC MRI

The effect of the eddy-current correction on the CD images can be seen by visually comparing uncorrected and corrected images of all four TRU-PC scans (Figure 2a). The artifactual tissue signal is minimal in the large vessel protocol (lAP, lFH), but becomes prominent in the small vessel protocols (sAP, sFH) due to increased gradient strength. It is also evident from the four hyperplanes (middle column, Figure 2a) that the eddy-current induced phase is dependent on the flow encoding direction.

Shown in Figure 2b are representative uncorrected and corrected T_2 maps, and the corresponding Y_v maps. In regions of eddy-current induced phase error (white arrows in Figure 2b), the T_2 cannot be accurately estimated in the uncorrected image, but is modified upon removal of the artifact, which then falls into a more physiologically meaningful range. The T_2 differences directly translate to Y_v differences. Averaging across the entire brain, the T_2 before correction (80.2±7.7ms) is significantly higher than after correction (74.2±8.3%), (P=0.006). Similarly, the average Y_v before correction (69.0±3.3%) is significantly higher than the Y_v after correction (66.4±3.8%), (P=0.006). Each subject's average T2 and Yv values before and after correction are reported in Table 1. The significance between uncorrected and corrected T2 (or Yv) values was tested with a two-tailed paired Student's t-test.

Although the general trend is that the eddy-currents cause T_2 to become longer (i.e. ΔT_2 is positive), some voxels manifested the opposite effect. Numerical simulation was therefore performed to understand this observation. Figure 3a shows simulation results, which

describe the effects of eddy-currents on blood T_2 estimation. When the eddy-current induced phase $\Delta\varepsilon$ is positive, the T_2 is overestimated, and when $\Delta\varepsilon$ is negative, the T_2 is underestimated.

This simulation result is confirmed by the in vivo data. Figures 3b and c showed scatter plots between $\Delta T2$ and $\Delta\varepsilon$ from various ROIs on the TRU-PC small vessel scans, for AP (Figure 3b, R=0.6842, $P<0.0001$) and FH (Figure 3c, R=0.8758, $P<0.0001$) flow-encoding direction, respectively.

Reproducibility and sensitivity to caffeine challenge

Test-retest reproducibility of (corrected) Y_v maps is shown in Figure 4 for all five subjects. The good visual agreement between repetition 1 and 2 is promising. Quantitatively, the proposed mapping method is relatively stable, with an average voxel-wise CoV of 3.7±1.2%. Linear regression of the voxel-wise $R_2(=1/T_2)$ relationship between repetition 1 and 2 also shows good agreement (slope=1.03). Table 2 documents the average Yv values for repetition 1 and 2, before and after eddy-current correction.

In an additional five subjects, the sensitivity to a caffeine challenge was tested. The (corrected) Y_v-maps at baseline and after caffeine ingestion are shown in Figure 5, along with the difference images. As expected, the Y_v after caffeine ingestion is reduced (including the pial vessels), suggesting excellent sensitivity to physiological changes. The average voxel-wise Y_v is significantly lower ($P<0.001$) after caffeine ingestion (54.7±4.6%) compared to baseline (66.4±3.7%), resulting in an average voxel-wise Y_v difference of 11.6±2.4%. Table 3 documents the average Yv values for baseline and caffeine conditions, before and after eddy-current correction.

Finally, we examined whether Y_v measured in small vessels are consistent with that in large vessels. Before eddy-current correction, the small vessel Y_v was observed to be greater than the Y_v of the large vessels (Figure 6b). After correction, the small vessel Y_v matches the large vessel Y_v with a close to unity relationship (Figure 6c, slope=1.08, R=0.9671, $P<0.001$), again suggesting that the proposed eddy-current correction scheme promotes a more accurate Y_v measurement.

Discussion

The present work is a follow-up study of a recently proposed technique, T2-Relaxation-Under-Phase-Contrast (TRU-PC). The proof-of-principle of this technique was shown independently by two groups, Krishnamurthy et al. (30) and Jain et al. (13), but primarily focused on large veins using a Venc of 15-20 cm/sec. The present study aims to push the envelope of this technique for the measurement of oxygenation in small veins (using a low Venc of 3 or 5 cm/sec). At this velocity range, we found that the strong flow-encoding gradients generated eddy-currents, resulting in an incomplete cancellation of static tissue. The presence of static tissue in the venogram can compromise the evaluation of blood oxygen saturation, resulting in either an under- or over-estimation of Yv. Therefore, we sought to optimize and correct the TRU-PC images during post-processing to recover an accurate Yv of small, slow-flowing veins. While the present study does not represent the

contribution of an original, completely new technique, we believe that the optimization of a recently developed technique is also valuable to receive wide adaptation and to direct it towards clinical application.

This study proposed a practical protocol to provide a voxel-by-voxel map of cerebral venous oxygenation in the human brain, with considerations of sensitivity to both major veins and small veins. Sequences tailored toward small veins tend to generate considerable eddy-currents effects. Thus, a correction method was proposed and its efficacy was demonstrated with simulations and in vivo experiments. The optimized protocol was tested in terms of its reproducibility and ability to detect known oxygenation-altering challenges.

Motivation for vessel-specific Y_v measurements

Several studies have shown that whole-brain oximetry techniques (12,17,47,48) provide a robust estimation of cerebral oxygenation and metabolic rate, but inherently lack spatial specificity. A “vessel-specific” imaging technique will instead promote a more regional measurement of Y_v and $CMRO_2$.

Anticipating such a need, we previously showed the feasibility of the TRU-PC technique to small draining vessels (30). However, based on our imaging technique at that time, we were only able to provide ROI Y_v values, and only vessels with a predefined flow direction were detectable. With the new mapping technique presented in this paper, we are now able to produce a map of the entire mid-sagittal vasculature with arbitrary flow direction, including small draining veins.

Comparison with other vessel-specific Y_v techniques

Recently, another group has also proposed vessel-specific Y_v measures with Quantitative Susceptibility Mapping (QSM) (25). QSM directly quantifies the susceptibility of a voxel by finding the source of the measured fields (49). By relating the susceptibility with the amount of deoxyhemoglobin, the Y_v of a venous segment can be estimated with QSM.

The QSM-Y_v technique produces realistic 3D representations of the brain's volumetric venous vasculature, but we believe that TRU-PC MRI might offer several advantages compared to the QSM technique. For one, unlike QSM, TRU-PC does not require the empirical choice of a reference tissue, which could unintentionally bias the QSM-Y_v measurement. It has also been shown that the presence of flow could impact the reconstruction of the field map used in the QSM-Y_v quantification (50). Since blood is intrinsically flowing, an immediate bias will be observed in the QSM technique, and must be recovered with mathematical modeling. The T_2 measurements in TRU-PC are not influenced by flow because the non-slice-selective CPMG T_2-preparation is stable in the presence of flow (51).

On the other hand, TRU-PC requires the blood to be flowing, and may not be able to register vessels that have little or no flow. Conditions of low flow could arise in disease states, such as infarction or venous thrombosis (52). In this case, QSM-Y_v would be superior to TRUPC, in that it could register the presence of low-velocity blood. Thus, the choice of Y_v measurement technique depends on specific clinical population of interest.

Eddy-current induced phase errors

The presence of eddy-currents in small vessel scans is a nuisance that could lead to gross Y_v quantification errors (range of −22.6% to 37.5%, average of 2.6%). The phenomenon is diminished in large vessel scans, simply because the flow-encoding gradients are smaller. The use of a second order polynomial to estimate eddy-currents was predicted by Bernstein, et al (36), and has been successfully used to correct PC MRI data (53). With the simple formulation proposed by Langham, et al (37), we showed that the correction effectively removes the phase error due to eddy-currents, and improves the Y_v quantification accuracy.

Langham, et al. applied their technique to gradient echo images, and phase-based oximetry measurements. In this study, we have expanded upon Langham, et al.'s work, and applied their technique to Phase Contrast MRI to correct a T2-based oximetry technique. Thus, we have appropriately tailored our study towards the effects of eddy-currents on T2 measurements using TRU-PC. Most methods remove eddy-current induced phase in vessels based on ROIs of adjacent static tissue (54). However, this is susceptible to biases induced by subjective ROI selections and is not practical for voxel-by-voxel mapping studies. The method of fitting a hyperplane takes into account the eddy-current pattern over the entire image, and is less labor-intensive.

Practical considerations in the proposed TRU-PC protocol

One challenge of mapping the entire vasculature is maintaining reasonable scan durations. The proposed TRU-PC protocol includes four separate scans (large and small vessels with AP and FH flow-encoding directions), thus the total scan duration could be greater than 30 minutes if no other adjustments are made. We therefore made several changes to reduce the scan duration. One is that we reduced the number of eTEs acquired, from the original 3 to 2. The longest TE value in the previous protocol was removed. In principle, the lower number of data points (eTEs) could reduce the fitting reliability. In practice, we found that the CoV of 3.7±1.2% is similar to the previously reported CoV of 3.5±1.0% (30). This may be because 1) the longer eTE data are noisy to start with; 2) the average of four difference scans could recover some of the data stability. We also slightly reduced the image resolution in the phase-encoding direction, thereby further shortening the scan duration. The lower resolution means that more static tissue spins would contribute to the voxel signal measured. But the use of the flowing-encoding gradients should be able to preserve only the blood signal in the final Complex-Difference image. With these improvements, the total duration of the proposed TRU-PC protocol is 13min and 20sec.

Limitations of the study

We note that additional measurement bias could stem from a sub-optimal T_2-prep, especially in the presence of B_1 inhomogeneity. Simulations show that a 10% error in B_1, could bias the T_2 values as much as 2.5ms, which translates to a Y_v bias of 1.1% (assuming T_2=75ms, Hct=41%). Thus, it is important for T_2-based oximetry to have a robust preparation of the magnetization. This can be controlled experimentally through adiabatic refocusing (51) or B_1 shimming (55).

The phase errors removed with the hyperplane have been attributed to eddy-currents, but may also contain some contribution from concomitant fields. In our image reconstruction, we did not calculate the concomitant fields, which could be considered a limitation. Methods have been described that calculate the precise amount of concomitant fields based on the pulse sequence, the gradient geometry, and the position of each voxel from the isocenter (36). It would be ideal to disentangle the contribution from eddy-currents and concomitant fields, though the computations are resource intensive, and calculations are specific to each scanner. Thus, to maintain a generic algorithm, we chose to remove all phase errors with the hyperplane, and generalize them to eddy-current induced phase errors.

Another limitation of this study is that hematocrit was not measured, but rather assumed to be a uniform 41% across the entire vascular path. The T_2-Y_v conversion depends on Hct (29), and the Hct should ideally be measured. It is known that the hematocrit in the capillary bed is lower than the hematocrit in the large draining veins (46), but it is unknown in which vascular segment the Hct returns to the hematocrit measurable with a blood-draw. Since the diameter of the vessels in question (>1mm) are much larger than the diameter of a red blood cell (8μm) (56), we assume that the hematocrit does not change across the vessels that are visible with TRU-PC. Ideally, the Hct-T_1 relationship (40) could be exploited in a similar manner to measure the vessel-specific hematocrit for use in the T_2-Y_v conversion.

A major limitation of this study is that only a single mid-sagittal slice of the brain was acquired. Ideally, a whole-brain 3D coverage should be used to capture all veins of the brain. This was not feasible in this study due to scan duration limitations. The brain's anatomy has a highly symmetric organization, where most of the major draining vessels are positioned in the mid-sagittal, and the small vessels joining these veins are mostly visible in this plane as well. However, there are numerous other major draining veins (transverse sinus, sigmoid sinus, jugular vein, cavernous sinus, petrosal sinus, basal vein, superficial sylvian vein, trolard vein, etc.) that this study could not image, simply because we used a 2D single-slice acquisition scheme. Future studies should focus on expanding the coverage of TRU-PC acquisition, to include more vessels of the brain.

Conclusion

We have demonstrated that the mid-sagittal vessel-specific Y_v can be mapped on a voxelby-voxel basis with T_2-based oximetry. A procedure to remove eddy-currents induced artifact was used to correct the Y_v measurement. We demonstrated that the Y_v maps are reproducible and sensitive to physiological changes.

Acknowledgements

The authors thank Dr. Binu Thomas for his advice on using SPM.

Grant Sponsors: NIH R01 MH084021, NIH R01 NS067015, NIH R01 AG042753, NIH R21 NS078656, NIH R01 AG033106

References

1. Kety S, Schmidt C. The Effects of Altered Arterial Tension of Carbon Dioxide and Oxygen on Cerebral Blood Flow and Cerebral Oxygen Consumption of Normal Young Men. J Clin Invest. 1948; 27:484–492. [PubMed: 16695569]
2. Lu H, Xu F, Rodrigue KM, Kennedy KM, Cheng Y, Flicker B, Hebrank AC, Uh J, Park DC. Alterations in cerebral metabolic rate and blood supply across the adult lifespan. Cereb Cortex. 2011; 21(6):1426–1434. [PubMed: 21051551]
3. Peng SL, Dumas JA, Park DC, Liu P, Filbey FM, McAdams CJ, Pinkham AE, Adinoff B, Zhang R, Lu H. Age-related increase of resting metabolic rate in the human brain. Neuroimage. in press.
4. Liu P, Huang H, Rollins N, Chalak LF, Jeon T, Halovanic C, Lu H. Quantitative assessment of global cerebral metabolic rate of oxygen (CMRO2) in neonates using MRI. NMR Biomed. 2014; 27(3):332–340. [PubMed: 24399806]
5. Liu J, Zhu YS, Khan MA, Brunk E, Martin-Cook K, Weiner MF, Cullum CM, Lu H, Levine BD, Diaz-Arrastia R, Zhang R. Global brain hypoperfusion and oxygenation in amnestic mild cognitive impairment. Alzheimer's & dementia : the journal of the Alzheimer's Association. 2014; 10(2):162–170.
6. Ge Y, Zhang Z, Lu H, Tang L, Jaggi H, Herbert J, Babb JS, Rusinek H, Grossman RI. Characterizing brain oxygen metabolism in patients with multiple sclerosis with T2-relaxation-under-spin-tagging MRI. J Cereb Blood Flow Metab. 2012; 32(3):403–412. [PubMed: 22252237]
7. Liu P, Lu H, Filbey FM, Tamminga CA, Cao Y, Adinoff B. MRI assessment of cerebral oxygen metabolism in cocaine-addicted individuals: hypoactivity and dose dependence. NMR Biomed. 2014; 27(6):726–732. [PubMed: 24757009]
8. Mintun MA, Raichle ME, Martin WR, Herscovitch P. Brain oxygen utilization measured with O-15 radiotracers and positron emission tomography. J Nucl Med. 1984; 25(2):177–187. [PubMed: 6610032]
9. Oja JM, Gillen JS, Kauppinen RA, Kraut M, van Zijl PC. Determination of oxygen extraction ratios by magnetic resonance imaging. J Cereb Blood Flow Metab. 1999; 19(12):1289–1295. [PubMed: 10598932]
10. Golay X, Silvennoinen MJ, Zhou J, Clingman CS, Kauppinen RA, Pekar JJ, van Zij PC. Measurement of tissue oxygen extraction ratios from venous blood T(2): increased precision and validation of principle. Magn Reson Med. 2001; 46(2):282–291. [PubMed: 11477631]
11. Haacke EM, Lai S, Reichenbach JR, Kuppusamy K, Hoogenraad FG, Takeichi H, Lin W. In vivo measurement of blood oxygen saturation using magnetic resonance imaging: a direct validation of the blood oxygen level-dependent concept in functional brain imaging. Hum Brain Mapp. 1997; 5(5):341–346. [PubMed: 20408238]
12. Fernandez-Seara MA, Techawiboonwong A, Detre JA, Wehrli FW. MR susceptometry for measuring global brain oxygen extraction. Magn Reson Med. 2006; 55(5):967–973. [PubMed: 16598726]
13. Jain V, Magland J, Langham M, Wehrli FW. High temporal resolution in vivo blood oximetry via projection-based T(2) measurement. Magn Reson Med. 2013; 70(3):785–790. [PubMed: 23081759]
14. An H, Lin W. Quantitative measurements of cerebral blood oxygen saturation using magnetic resonance imaging. J Cereb Blood Flow Metab. 2000; 20(8):1225–1236. [PubMed: 10950383]
15. Qin Q, Grgac K, van Zijl PC. Determination of whole-brain oxygen extraction fractions by fast measurement of blood T(2) in the jugular vein. Magn Reson Med. 2011; 65(2):471–479. [PubMed: 21264936]
16. He X, Yablonskiy DA. Quantitative BOLD: mapping of human cerebral deoxygenated blood volume and oxygen extraction fraction: default state. Magn Reson Med. 2007; 57(1):115–126. [PubMed: 17191227]
17. Lu H, Ge Y. Quantitative evaluation of oxygenation in venous vessels using T2- Relaxation-Under-Spin-Tagging MRI. Magn Reson Med. 2008; 60(2):357–363. [PubMed: 18666116]

18. Bolar DS, Rosen BR, Sorensen AG, Adalsteinsson E. QUantitative Imaging of eXtraction of oxygen and TIssue consumption (QUIXOTIC) using venular-targeted velocity- selective spin labeling. Magn Reson Med. 2011; 66(6):1550–1562. [PubMed: 21674615]
19. Guo J, Wong EC. Venous oxygenation mapping using velocity-selective excitation and arterial nulling. Magn Reson Med. 2012; 68(5):1458–1471. [PubMed: 22294414]
20. Gauthier CJ, Hoge RD. Magnetic resonance imaging of resting OEF and CMRO(2) using a generalized calibration model for hypercapnia and hyperoxia. Neuroimage. 2011; 60(2):1212–1225. [PubMed: 22227047]
21. Bulte DP, Kelly M, Germuska M, Xie J, Chappell MA, Okell TW, Bright MG, Jezzard P. Quantitative measurement of cerebral physiology using respiratory-calibrated MRI. Neuroimage. 2012; 60(1):582–591. [PubMed: 22209811]
22. Wise RG, Harris AD, Stone AJ, Murphy K. Measurement of OEF and absolute CMRO2: MRI-based methods using interleaved and combined hypercapnia and hyperoxia. Neuroimage. 2013; 83:135–147. [PubMed: 23769703]
23. Haacke EM, Tang J, Neelavalli J, Cheng YC. Susceptibility mapping as a means to visualize veins and quantify oxygen saturation. J Magn Reson Imaging. 2010; 32(3):663–676. [PubMed: 20815065]
24. Fan AP, Benner T, Bolar DS, Rosen BR, Adalsteinsson E. Phase-based regional oxygen metabolism (PROM) using MRI. Magn Reson Med. 2012; 67(3):669–678. [PubMed: 21713981]
25. Fan AP, Bilgic B, Gagnon L, Witzel T, Bhat H, Rosen BR, Adalsteinsson E. Quantitative oxygenation venography from MRI phase. Magn Reson Med. 2014; 72(1):149–159. [PubMed: 24006229]
26. Wright GA, Hu BS, Macovski A. 1991 I.I. Rabi Award. Estimating oxygen saturation of blood in vivo with MR imaging at 1.5 T. J Magn Reson Imaging. 1991; 1(3):275–283. [PubMed: 1802140]
27. Thulborn KR, Waterton JC, Matthews PM, Radda GK. Oxygenation dependence of the transverse relaxation time of water protons in whole blood at high field. Biochim Biophys Acta. 1982; 714(2):265–270. [PubMed: 6275909]
28. Zhao JM, Clingman CS, Narvainen MJ, Kauppinen RA, van Zijl PC. Oxygenation and hematocrit dependence of transverse relaxation rates of blood at 3T. Magn Reson Med. 2007; 58(3):592–597. [PubMed: 17763354]
29. Lu H, Xu F, Grgac K, Liu P, Qin Q, van Zijl P. Calibration and validation of TRUST MRI for the estimation of cerebral blood oxygenation. Magn Reson Med. 2012; 67(1):42–49. [PubMed: 21590721]
30. Krishnamurthy LC, Liu P, Ge Y, Lu H. Vessel-specific quantification of blood oxygenation with T2-relaxation-under-phase-contrast MRI. Magn Reson Med. 2014; 71(2):978–989. [PubMed: 23568830]
31. Moran PR. A flow velocity zeugmatographic interlace for NMR imaging in humans. Magn Reson Imaging. 1982; 1(4):197–203. [PubMed: 6927206]
32. Bryant DJ, Payne JA, Firmin DN, Longmore DB. Measurement of flow with NMR imaging using a gradient pulse and phase difference technique. J Comput Assist Tomogr. 1984; 8(4):588–593. [PubMed: 6736356]
33. Pelc NJ, Bernstein MA, Shimakawa A, Glover GH. Encoding strategies for three- direction phase-contrast MR imaging of flow. J Magn Reson Imaging. 1991; 1(4):405–413. [PubMed: 1790362]
34. Carr HY, Purcell EM. Effects of Diffusion on Free Precession in Nuclear Magnetic Resonance Experiments. Phys Rev. 1954; 94(3):630–638.
35. Meiboom S, Gill D. Modified Spin-Echo Method for Measuring Nuclear Relaxation Times. The Review of Scientific Instruments. 1958; 29(8):688–691.
36. Bernstein MA, Zhou XJ, Polzin JA, King KF, Ganin A, Pelc NJ, Glover GH. Concomitant gradient terms in phase contrast MR: analysis and correction. Magn Reson Med. 1998; 39(2):300–308. [PubMed: 9469714]
37. Langham MC, Magland JF, Floyd TF, Wehrli FW. Retrospective correction for induced magnetic field inhomogeneity in measurements of large-vessel hemoglobin oxygen saturation by MR susceptometry. Magn Reson Med. 2009; 61(3):626–633. [PubMed: 19107914]

38. Bernstein MA, Grgic M, Brosnan TJ, Pelc NJ. Reconstructions of phase contrast, phased array multicoil data. Magn Reson Med. 1994; 32(3):330–334. [PubMed: 7984065]
39. Lu H, Nagae-Poetscher LM, Golay X, Lin D, Pomper M, van Zijl PC. Routine clinical brain MRI sequences for use at 3.0 Tesla. J Magn Reson Imaging. 2005; 22(1):13–22. [PubMed: 15971174]
40. Lu H, Clingman C, Golay X, van Zijl PC. Determining the longitudinal relaxation time (T1) of blood at 3.0 Tesla. Magn Reson Med. 2004; 52(3):679–682. [PubMed: 15334591]
41. Levitt MH, Freeman R, Frenkiel T. Broadband Heteronuclear Decoupling. J Magnetic Res. 1982; 47:328–330.
42. Haacke EM, Xu Y, Cheng YC, Reichenbach JR. Susceptibility weighted imaging (SWI). Magn Reson Med. 2004; 52(3):612–618. [PubMed: 15334582]
43. Pruessmann KP, Weiger M, Scheidegger MB, Boesiger P. SENSE: sensitivity encoding for fast MRI. Magn Reson Med. 1999; 42(5):952–962. [PubMed: 10542355]
44. Mulderink TA, Gitelman DR, Mesulam MM, Parrish TB. On the use of caffeine as a contrast booster for BOLD fMRI studies. Neuroimage. 2002; 15(1):37–44. [PubMed: 11771972]
45. Haacke EM, Mittal S, Wu Z, Neelavalli J, Cheng YC. Susceptibility-weighted imaging: technical aspects and clinical applications, part 1. AJNR Am J Neuroradiol. 2009; 30(1):19–30. [PubMed: 19039041]
46. Oldendorf WH, Kitano M, Shimizu S, Oldendorf SZ. Hematocrit of the human cranial blood pool. Circulation research. 1965; 17(6):532–539. [PubMed: 5843886]
47. Liu P, Xu F, Lu H. Test-retest reproducibility of a rapid method to measure brain oxygen metabolism. Magn Reson Med. 2013; 69(3):675–681. [PubMed: 22517498]
48. Jain V, Langham MC, Wehrli FW. MRI estimation of global brain oxygen consumption rate. J Cereb Blood Flow Metab. 2010; 30(9):1598–1607. [PubMed: 20407465]
49. Schweser F, Deistung A, Lehr BW, Reichenbach JR. Differentiation between diamagnetic and paramagnetic cerebral lesions based on magnetic susceptibility mapping. Medical physics. 2010; 37(10):5165–5178. [PubMed: 21089750]
50. Xu B, Liu T, Spincemaille P, Prince M, Wang Y. Flow compensated quantitative susceptibility mapping for venous oxygenation imaging. Magn Reson Med. in press.
51. Jenista ER, Rehwald WG, Chen EL, Kim HW, Klem I, Parker MA, Kim RJ. Motion and flow insensitive adiabatic T2-preparation module for cardiac MR imaging at 3 Tesla. Magn Reson Med. 2013; 70(5):1360–1368. [PubMed: 23213005]
52. Wasay M, Azeemuddin M. Neuroimaging of cerebral venous thrombosis. Journal of neuroimaging : official journal of the American Society of Neuroimaging. 2005; 15(2):118–128. [PubMed: 15746223]
53. Lorenz R, Bock J, Snyder J, Korvink JG, Jung BA, Markl M. Influence of eddy current, Maxwell and gradient field corrections on 3D flow visualization of 3D CINE PC-MRI data. Magn Reson Med. 2014; 72(1):33–40. [PubMed: 24006013]
54. Bernstein, MA.; King, KF.; Zhou, XJ. Phase Contrast: Handbook of MRI Pulse Sequences. Elsevier Academic Press; Burlington, MA: 2004.
55. Mao W, Smith MB, Collins CM. Exploring the limits of RF shimming for high-field MRI of the human head. Magn Reson Med. 2006; 56(4):918–922. [PubMed: 16958070]
56. Pries AR, Secomb TW, Gaehtgens P. Biophysical aspects of blood flow in the microvasculature. Cardiovasc Res. 1996; 32(4):654–667. [PubMed: 8915184]

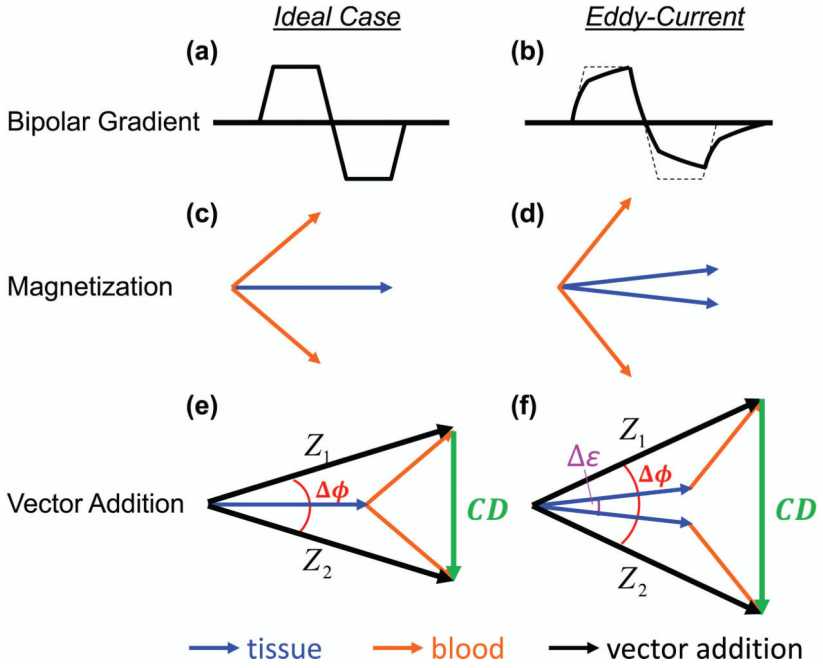

Figure 1.

The resulting magnetization vectors in response to Phase Contrast (PC) MRI for the ideal case, and the case of eddy-currents. The ideal bipolar gradient is shown in (a). In (b) the bipolar gradient has been distorted by the presence of eddy-currents. (c) The ideal tissue magnetization (blue vector, overlapping between two schemes) and blood magnetization (orange vector) resulting from the positive and negative bipolar gradient schemes. (d) Eddy-currents cause the tissue and blood magnetizations to accumulate additional phase. (e) The vector addition (black arrow) of tissue and blood magnetization for the ideal case, given by Z_1 and Z_2, and the Complex Difference (CD) vector (green arrow), which only contains information from blood. (f) In the presence of eddy-currents, incomplete subtraction of the tissue vectors causes the CD to contain information from both blood and tissue. The quantity $\delta\varphi$ is the measured phase difference between Z_1 and Z_2. The quantity $\delta\varepsilon$ is the phase error induced by eddy-currents.

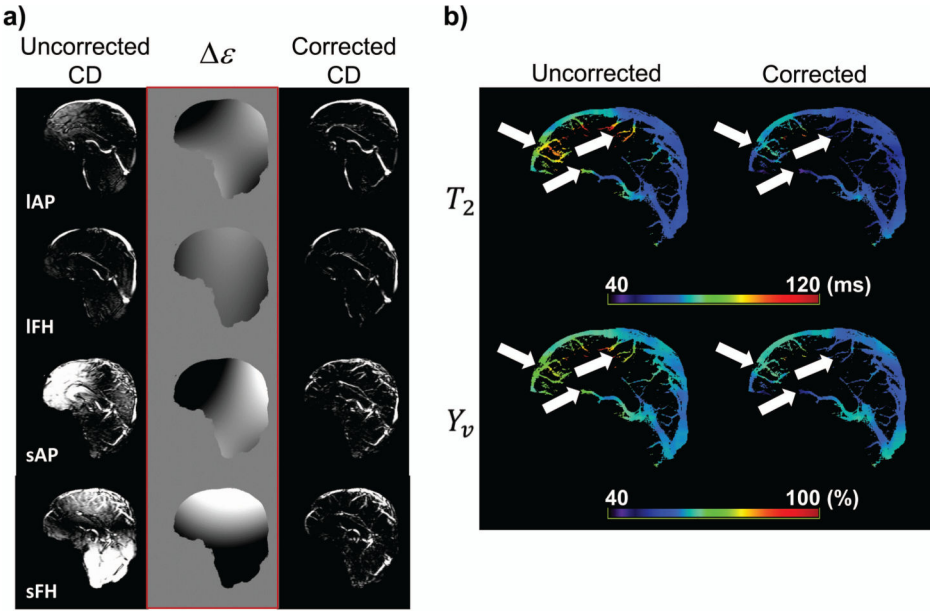

Figure 2.

The effect of eddy-current correction. (a) A set of representative uncorrected and corrected CD images, as well as the Δε hyperplane calculated for the correction algorithm. Shown are the eTE=0ms images for all four TRU-PC scans (sensitized to different flow directions and blood velocities). lAP: large vessel in Anterior-Posterior, lFH: large vessel in Foot-Head, sAP: small vessel in Anterior-Posterior, sFH: small vessel in Foot-Head. (b) The uncorrected and corrected T_2 maps (in ms), and respective Y_v maps (in %). The eddy-current correction modifies the T_2 and Y_v (white arrows).

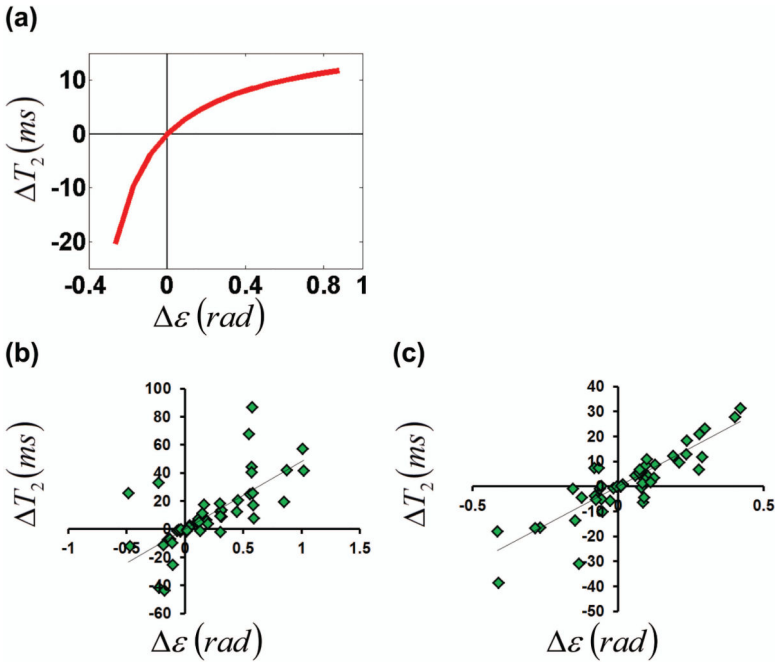

Figure 3.

Effects of eddy-current correction on blood T_2 estimation. (a) Bloch simulation: the amount of blood T_2 correction is related to the amount of eddy-current induced phase error. (b) In vivo: the T_2-Δε relationship in AP. (c) In vivo: the T_2-Δε relationship in FH. Both flow-encoding directions mimic the relationship predicted in (a).

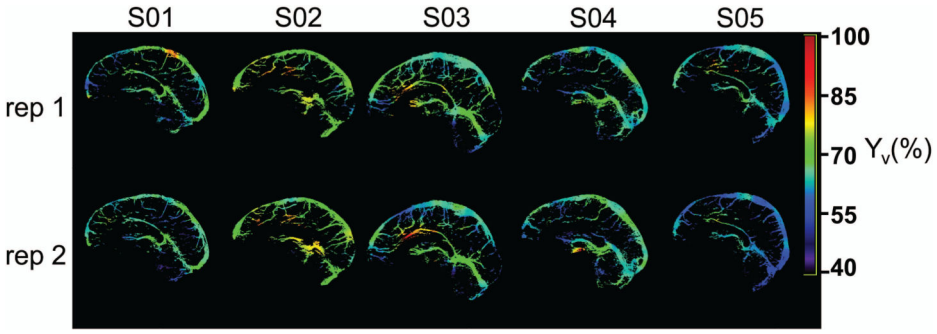

Figure 4.
Test-retest reproducibility of corrected Y_v maps (in %) for five subjects.

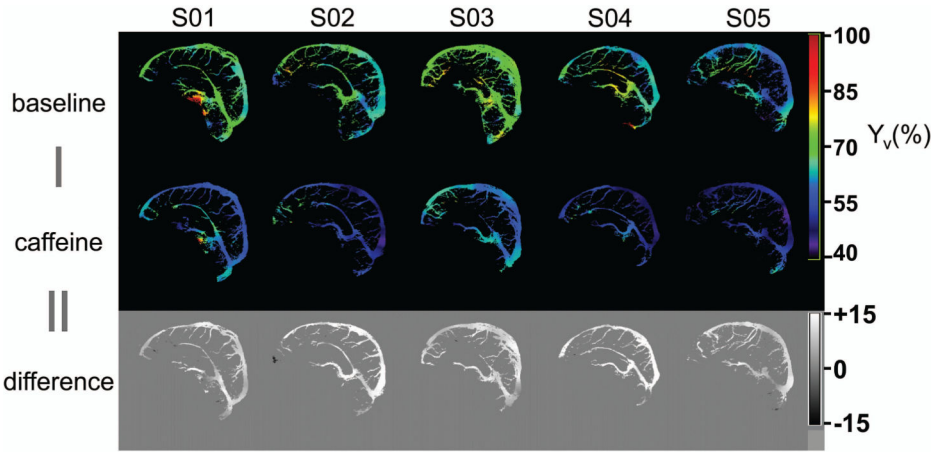

Figure 5.

Corrected Y_v maps (in %) at baseline and after ingestion of caffeine for five subjects, along with voxel-wise difference maps (in %).

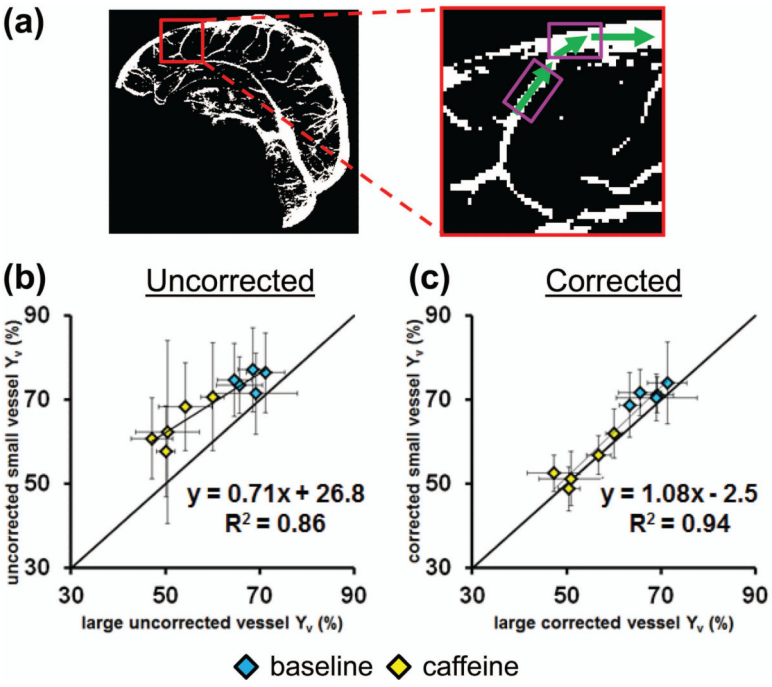

Figure 6.

The relationship between measured Y_v in adjacent small and large vessels. (a) A representative vessel mask with zoomed inset shows that the blood from small vessels will travel into the adjacent large vessel segment. The pink boxes show sample ROI selections to probe the relationship between small vessels and large vessels. The relationship (b) before, and (c) after eddy-current correction for baseline (blue diamonds) and after ingestion of caffeine (yellow diamonds) (N=5). The error bars represent standard deviation across 10 Y_v values (5 from Anterior-Posterior scans, 5 from Foot-Head scans).

Table 1

The effect of eddy-current correction on average T2 and Yv values.

Subject	T2 (ms) (uncorrected)	T2 (ms) (corrected)	Yv (%) (uncorrected)	Yv (%) (corrected)
S01	*81.8*	*73.8*	*69.7*	*66.3*
S02	*89.2*	*86.8*	*72.8*	*71.9*
S03	*83.9*	*75.3*	*70.6*	*66.9*
S04	*77.2*	*71.5*	*67.8*	*65.4*
S05	*68.8*	*63.7*	*63.9*	*61.4*
Average ± Stdev	**80.2 ± 7.7**	**74.2 ± 8.3**	**69.0 ± 3.3**	**66.4 ± 3.8**
P-value (paired t-test)	*P=0.006*		*P=0.006*	

Table 2

The effect of eddy-current correction on average Yv values, for repetition 1 and 2.

Subject	Repetition 1		Repetition 2	
	Yv (%) (uncorrected)	Yv (%) (corrected)	Yv (%) (uncorrected)	Yv (%) (corrected)
S01	*70.0*	*67.3*	*69.3*	*65.2*
S02	*72.4*	*71.9*	*73.2*	*72.0*
S03	*70.8*	*67.3*	*70.4*	*66.6*
S04	*67.2*	*65.0*	*68.5*	*65.8*
S05	*65.8*	*63.4*	*62.0*	*59.4*
Average ± Stdev	**69.2 ± 2.7**	**67.0 ± 3.2**	**68.7 ± 4.1**	**65.8 ± 4.5**

Table 3

The effect of eddy-current correction on average Yv values, for baseline and caffeine conditions.

Subject	Baseline		Caffeine	
	Yv (%) (uncorrected)	Yv (%) (corrected)	Yv (%) (uncorrected)	Yv (%) (corrected)
S01	*70.4792*	*68.3725*	*64.1458*	*58.8990*
S02	*67.7939*	*65.7894*	*57.4593*	*52.0917*
S03	*72.8162*	*70.8012*	*63.6802*	*60.4533*
S04	*68.7396*	*66.1960*	*55.8583*	*51.4197*
S05	*65.2361*	*60.7926*	*57.4959*	*50.8798*
Average ± Stdev	**69.0 ± 2.8**	**66.4 ± 3.7**	**59.7 ± 3.9**	**54.7 ± 4.6**